

Plan Nacional de Nuevos Materiales.

### Appendix: Computational Details

Electronic band structure calculations<sup>11</sup> within the extended Hückel framework<sup>12</sup> were performed for different geometries on the model compounds listed below. Extended Hückel parameters<sup>18,43</sup> employed in our calculations are collected in Table III.

For singly bridged compounds, the following models were used:  $[\text{CuCl}_3(\mu\text{-Cl})]^{2-}_n$  (structure 1, with  $120^\circ < \delta < 180^\circ$  and  $90^\circ < \varphi < 150^\circ$ , at intervals of  $10^\circ$ ; structure 2 with  $90^\circ < \varphi < 120^\circ$  and  $\delta = 360^\circ - 2\varphi$ ) and  $[\text{CuBr}_3(\mu\text{-Br})]^{2-}_n$  (structure 1 with  $120^\circ < \delta < 180^\circ$  and  $90^\circ < \varphi < 150^\circ$ , at intervals of  $10^\circ$ ). The following bond distances were used: Cu-X (short) = 2.3 and 2.4 Å, Cu-X (long) =

2.7, 2.8 Å for X = Cl and Br, respectively. For doubly bridged chains, calculations were carried out using  $[\text{CuCl}_2(\mu\text{-Cl})_2]^{2-}_n$  as a model (structures 3-5, with  $72^\circ < \varphi < 108^\circ$  at intervals of  $2^\circ$ ), with the following bond distances: Cu-Cl (short) = 2.3 Å, and Cu-X (long) = 2.8, 3.0, and 3.2 Å. For the molecular calculations on a dimer  $[\text{CuBr}_4(\mu\text{-Br})_2]^{6-}$  (Figure 4, bottom), we used bromide as a bridging ligand instead of chloride, and the long Cu-X bond distance was reduced to 2.6 Å, to exaggerate the overlap between the neighboring HOMOs of the dinuclear complex; in that way one can compensate for the neglect of the extended interactions which are taken into account in the band calculations. The bandwidths reported in Table I were calculated for the model compounds  $[\text{CuCl}_3(\mu\text{-X})]^{2-}_n$  with the experimental angles and the same bridging atom X as the real compound. Exchange coupling constants were calculated according to eq 2.

(43) Alvarez, S.; Mota, F.; Novoa, J. J. *Am. Chem. Soc.* **1987**, *109*, 6586.

## Kinetics and Mechanism of the Crystallization of $\text{Mg}_2\text{Al}_4\text{Si}_5\text{O}_{18}$ (Cordierite) from $\text{MgAl}_2\text{O}_4$ and $\text{SiO}_2$ in the Presence of a Bismuth Oxide Flux

Ryan W. Dupon, Adam C. Tanous, and Mark S. Thompson\*

Corporate R&D, Raychem Corporation, 300 Constitution Dr., Menlo Park, California 94025

Received May 11, 1990

Quantitative kinetics and a mechanistic interpretation are presented for the reaction of colloidal  $\text{SiO}_2$  and  $\text{MgAl}_2\text{O}_4$  to give  $\text{Mg}_2\text{Al}_4\text{Si}_5\text{O}_{18}$  in the presence of 2 atom % bismuth oxide. The active flux agent appears to be comprised predominantly of bismuth oxide and silicon oxide. The reaction proceeds through dissolution of the  $\text{MgAl}_2\text{O}_4$  in the siliceous flux to produce an aluminum-substituted quartz stuffed with magnesium ions as an intermediate. The stuffed quartz then converts to cordierite by a first-order process. The rate constant for this conversion is  $4.4 \times 10^{-5} \text{ s}^{-1}$  at  $1000^\circ \text{C}$  with an activation energy of 70 kcal/mol.

### Introduction

The preparation of cordierite ( $\text{Mg}_2\text{Al}_4\text{Si}_5\text{O}_{18}$ ) ceramics has attracted considerable attention due in large part to the small thermal expansion coefficient, good strength, and low dielectric constant of  $\text{Mg}_2\text{Al}_4\text{Si}_5\text{O}_{18}$ . Reported preparation methodologies have included the crystallization of glasses with the cordierite composition<sup>1-5</sup> and the hydrolysis of mixed, reactive intermediates such as metal alkoxides<sup>6-8</sup> with the cordierite composition followed by crystallization to the cordierite phase. The conversion mechanism from starting materials to cordierite for each of these processes has been investigated in some detail. Schreyer and Schairer have performed a comprehensive study of the observed phases in the crystallization of glasses in the  $\text{MgO-Al}_2\text{O}_3\text{-SiO}_2$  system around the composition of cordierite.<sup>1</sup> Chowdry<sup>7</sup> and Bernier et al.<sup>8</sup> have followed the conversion of hydrolyzed precursors to  $\text{Mg}_2\text{Al}_4\text{Si}_5\text{O}_{18}$  by X-ray diffraction. As preparative processes both the glass crystallization and sol-gel route have some drawbacks. The glass crystallization process uses common oxide starting materials but requires high temperatures and is inherently a two-step process. The sol-gel process uses expensive, high-energy intermediates, which makes it an expensive and impractical route for bulk oxide materials. We recently reported the preparation of  $\text{Mg}_2\text{-}$

$\text{Al}_4\text{Si}_5\text{O}_{18}$  below  $1000^\circ \text{C}$  by the reaction of  $\text{SiO}_2$  with  $\text{MgAl}_2\text{O}_4$  in the presence of a small amount of a bismuth oxide flux,<sup>9</sup> while in the absence of bismuth oxide there is no observed reaction. In that paper we described several

(1) Schreyer, W.; Schairer, J. F. Metastable Solid Solutions with Quartz-Type Structures on the Join  $\text{SiO}_2\text{-MgAl}_2\text{O}_4$ . *Z. Kristallogr.* **1961**, *116*, 60-82.

(2) Gregory, A. G.; Vearey, T. J. The Crystallization of Cordierite Glass. *J. Mater. Sci.* **1971**, *6*, 1312-21.

(3) Zdaniewski, W. "DTA and X-ray Analysis Study of Nucleation and Crystallization of  $\text{MgO-Al}_2\text{O}_3\text{-SiO}_2$  Glasses Containing  $\text{ZrO}_2$ ,  $\text{TiO}_2$ , and  $\text{CeO}_2$ ." *J. Am. Ceram. Soc.* **1975**, *58*, 163-69.

(4) Bridge, D. R.; Holland, D.; McMillan, P. W. Development of the Alpha-Cordierite Phase in Glass Ceramics for Use in Electronic Devices. *Glass Technol.* **1985**, *26*, 286-92.

(5) Watanabe, K.; Giess, E. Coalescence and Crystallization in Powdered High-cordierite ( $2\text{MgO} \cdot 2\text{Al}_2\text{O}_3 \cdot 5\text{SiO}_2$ ) Glass. *J. Am. Ceram. Soc.* **1985**, *68*, C-102-3.

(6) Moyer, J. R.; Prunier, A. R.; Hughes, N. N.; Winterton, R. C. *Mater. Res. Soc. Symp. Proc.* **1986**, *73*, 117-21.

(7) Gensse, C.; Chowdry, U. Non-Conventional Routes to Glass-Ceramics for Electronic Packaging. *Mater. Res. Soc. Symp. Proc.* **1986**, *73*, 693-703.

(8) Bernier, J. C.; Vilminot, S.; Rehspringer, J. L.; El Hadigui, S.; Poix, P. Sol-Gel Processes and Synthesis of Dielectric Powders for Multilayer Ceramics. *High Tech Ceramics*; Vincenzini, P., Ed.; Elsevier: Amsterdam, 1987; pp 1443-50.

(9) Dupon, R. W.; McConville, R. L.; Musolf, D. J.; Tanous, A. C.; Thompson, M. S. Preparation of Cordierite below  $1000^\circ \text{C}$  via Bismuth Oxide Flux. *J. Am. Ceram. Soc.* **1990**, *73*, 335-339.

(10) JCPDS file no. 12-708.

(11) Perry, R. H.; Chilton, C. H., Eds.; *Chemical Engineers Handbook*, 5th ed.; McGraw Hill: New York, 1973; Vol. 3-247.

\* To whom correspondence should be addressed.

distinctive features of that reaction. It was observed that there was an induction period before the appearance of cordierite that was both temperature and bismuth oxide concentration dependent. Further, the induction period went to infinity at around 960 °C, below which temperature no cordierite was formed. As the presence of bismuth oxide provides unique reaction paths to convert simple oxides to useful materials such as cordierite, it was of interest to us to follow the phase evolution of this reaction in an attempt to understand why the bismuth oxide exerts such a strong influence on the reaction of these oxides. Additionally, we sought to obtain quantitative kinetic information on the reactions and phase transformations as they occurred. Quantitative kinetic analyses are not typically done of reactions in the solid state; however, such information could be valuable to advancing the state of preparative art in oxide systems. To do this, an X-ray diffractometer was fitted with a platinum hot stage to enable the collection of time-dependent diffraction data near 1000 °C. The quantitative study of the kinetics for the reaction of colloidal SiO<sub>2</sub> with MgAl<sub>2</sub>O<sub>4</sub> to make Mg<sub>2</sub>Al<sub>4</sub>Si<sub>5</sub>O<sub>18</sub> in the presence of a bismuth oxide flux is presented in this paper.

### Experimental Section

**Powder Synthesis.** A more complete preparative description for this family of powders and resultant ceramics appears elsewhere.<sup>9</sup> The bismuth source used in these powders was a solution prepared by dissolving bismuth nitrate pentahydrate in nitric acid and diluting slowly with water until the bismuth ion concentration was 0.3 M and the nitrate concentration was 2.44 M. In a typical reaction, 0.05 mol (7.5 g) of colloidal SiO<sub>2</sub> was dispersed in 400 mL of deionized water along with 5 mL of ammonium hydroxide. An aliquot of 7.67 mL of the bismuth nitrate solution was added to the SiO<sub>2</sub> in base, resulting in a quantitative precipitation of the bismuth as a hydroxide. This was followed by the addition of 0.02 mol (2.85 g) of high surface area magnesium aluminate spinel to the bismuth hydroxide/silica dispersion, and the mixture was homogenized for 10 min with a high shear mixer. The solids were separated by filtration and calcined at 300 °C for 1 h. Following calcination of the powder, the temperature was increased to 1000 °C over the span of 30 min, held at this temperature for 1 min, and then removed from the oven. This brief exposure to 1000 °C does not change the observed phases present at 300 °C, but reduces the surface area and makes the powder easier to handle in the hot-stage X-ray analysis.

**High-Temperature XRD Description.** X-ray diffraction data were collected with an automated powder diffraction system<sup>12</sup> equipped with a high-temperature attachment.<sup>13</sup> The cordierite precursor powder was spread in a thin layer onto a resistively heated platinum band. A Pt/Pt 10% Rh thermocouple, spot-welded to the heating band, was used for temperature feedback to a Halder controller.<sup>14</sup> The sample was heated with a ramp of 20 °C/min to the reaction temperature and then held at that temperature until all measurements were completed. Diffraction data were collected by using Cu Kα<sub>1</sub> radiation (50 kV, 36 mA), a single-crystal germanium incident beam monochromator,<sup>15</sup> and a position sensitive detector.<sup>16</sup> The diffractometer was scanned from 9° to 39° 2θ at a speed of 2.5° 2θ/min after reaching the reaction temperature. Isothermal scans were repeated ever 20–60 min until the reaction was complete.

The raw data were subjected to a trend-oriented peak search to obtain peak positions and integrated intensities.

**Kinetics Determination.** All data for kinetic analyses were obtained by scanning repetitively at the desired temperature between 9° and 39°. Several peaks were selected for quantitative work. The peaks at 10.8° (100), 26.6° (112), 28.6° (202), and 29.6°

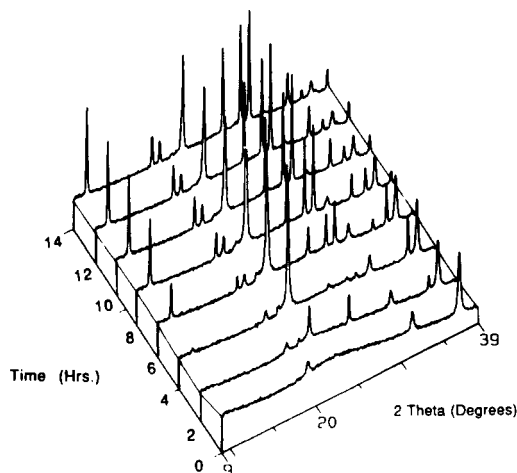


**Figure 1.** Time-dependent X-ray diffraction data at 1000 °C for the conversion of SiO<sub>2</sub> and MgAl<sub>2</sub>O<sub>4</sub> to Mg<sub>2</sub>Al<sub>4</sub>Si<sub>5</sub>O<sub>18</sub>.

(211) were used to follow the appearance of cordierite. The disappearance of the magnesium aluminate spinel was tracked at 36.7°. The presence of the SiO<sub>2</sub> intermediates β-cristobalite and the substitutionally modified quartz were monitored at 35.7° and 26.5°, respectively.

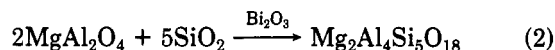
For rate constant calculations the integration of count intensity over angle 2θ (*I*) was used as an expression of concentration. Simple first-order rate law provided the best fit of the data and was used to determine a rate constant for the appearance of cordierite. By assuming a simple A to B reaction mechanism from a modified quartz intermediate (vide infra) to cordierite as shown in eq 1, the rate expression  $\ln(1 - I_t/I_\infty) = kt$  was derived and



used to determine first-order rate constants for the appearance of cordierite.

### Results and Discussion

The results of tracking the powder diffraction pattern as a function of time at 1000 °C from starting materials through Mg<sub>2</sub>Al<sub>4</sub>Si<sub>5</sub>O<sub>18</sub> formation appear in Figure 1:



Several features of these diffraction data should be noted. In the initial state (i.e., 1000 °C, *t* = 0), the only crystalline species present is MgAl<sub>2</sub>O<sub>4</sub>, as the SiO<sub>2</sub> used shows only an amorphous halo. As reported in the original paper,<sup>9</sup> there is an induction period of several hours at 1000 °C before crystalline Mg<sub>2</sub>Al<sub>4</sub>Si<sub>5</sub>O<sub>18</sub> begins to appear. By 12 h reaction time, the conversion to Mg<sub>2</sub>Al<sub>4</sub>Si<sub>5</sub>O<sub>18</sub> is complete and there are no other crystalline phases present. Two transient species are observed in the intermediate scans. The intermediate with the highest abundance indexes as β-cristobalite, and the less abundant intermediate best indexes as a substituted quartz phase.<sup>10</sup> Discussion of the significance of the presence of these intermediates is left until later in this paper.

To monitor the progress of the reaction and to allow the determination of reaction rates, plots of integrated peak intensity as a function of time for reflections of the spinel starting material, cordierite product, and both quartz intermediates were made. These plots are shown in Figure 3. Qualitatively, several features are apparent from these plots. The spinel begins to disappear immediately and then plateaus before resuming its disappearance. After some induction period β-cristobalite is observed to grow in, reach a maximum, and then disappear. The stuffed quartz also grows in and then disappears, but with an

(12) Siemens D-500.

(13) Anton Paar, K. G., P.O. Box 17, Graz, Austria.

(14) Halder Elektronik, Munich, FRG.

(15) Huber Diffraktionstechnik, D-8219 Rimsting, FRG.

(16) PSD-OED50M, Braun, Gutenbergstrasse 3, D-8046 Garching, FRG.

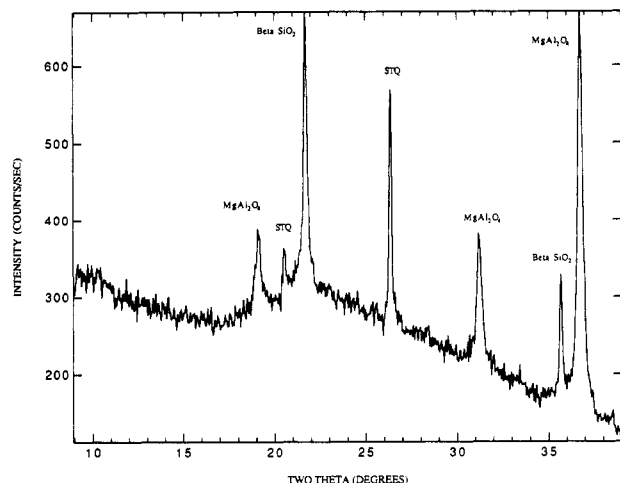


Figure 2. X-ray diffraction pattern of reaction intermediates at 1000 °C.

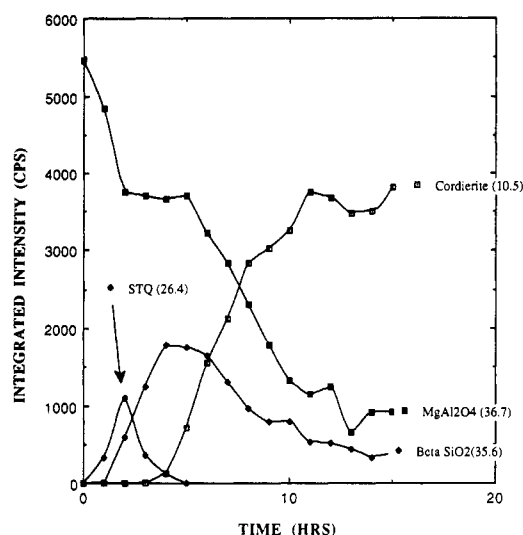


Figure 3. Integrated X-ray intensities for  $\text{Mg}_2\text{Al}_4\text{Si}_5\text{O}_{18}$ , cristobalite, stuffed quartz, and  $\text{MgAl}_2\text{O}_4$  as a function of time at 1000 °C.

Table I

$T, ^\circ\text{C}$	$2\theta, \text{deg } (hkl)$	$k, \text{s}^{-1}$	mean $k, \text{s}^{-1}$
975	10.8 (100)	$4.0 \times 10^{-5}$	$4.4 \times 10^{-5}$
	26.6 (112)	$4.7 \times 10^{-5}$	
	28.6 (202)	$4.7 \times 10^{-5}$	
	29.6 (211)	$4.2 \times 10^{-5}$	
1000	10.8 (100)	$9.5 \times 10^{-5}$	$9.9 \times 10^{-5}$
	26.6 (112)	$9.2 \times 10^{-5}$	
	28.6 (202)	$1.0 \times 10^{-4}$	
	29.6 (211)	$1.1 \times 10^{-4}$	
1025	10.8 (100)	$1.6 \times 10^{-4}$	$1.7 \times 10^{-4}$
	26.6 (112)	$1.9 \times 10^{-4}$	
	28.6 (202)	$1.5 \times 10^{-4}$	
	29.6 (211)	$1.8 \times 10^{-4}$	
1075	10.8 (100)	$2.4 \times 10^{-4}$	$3.8 \times 10^{-4}$
	26.6 (112)	$3.4 \times 10^{-4}$	
	28.6 (202)	$4.9 \times 10^{-4}$	
	29.6 (211)	$4.5 \times 10^{-4}$	

earlier maximum. Finally, the  $\text{Mg}_2\text{Al}_4\text{Si}_5\text{O}_{18}$  grows in smoothly after an induction period of several hours.

Using a first-order rate law, rate constants for the appearance of  $\text{Mg}_2\text{Al}_4\text{Si}_5\text{O}_{18}$  can be obtained from the integrated intensity vs time data. Typical first-order plots for  $\text{Mg}_2\text{Al}_4\text{Si}_5\text{O}_{18}$  appearance are shown in Figure 4. Rate constants for the reaction at 975, 1000, 1025, and 1075 °C appear in Table I. It can be observed that the rate con-

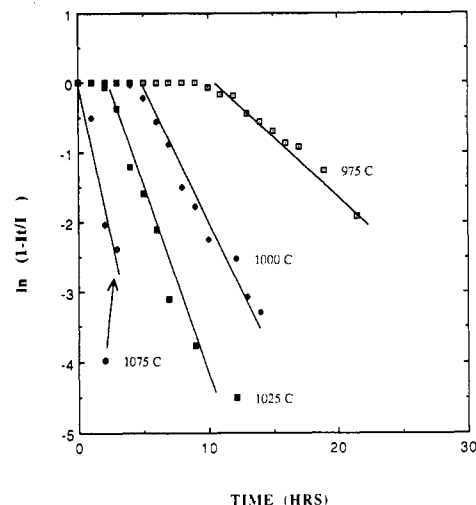


Figure 4. First-order kinetics plots for the appearance of  $\text{Mg}_2\text{Al}_4\text{Si}_5\text{O}_{18}$  at 975, 1000, 1025, and 1075 °C.

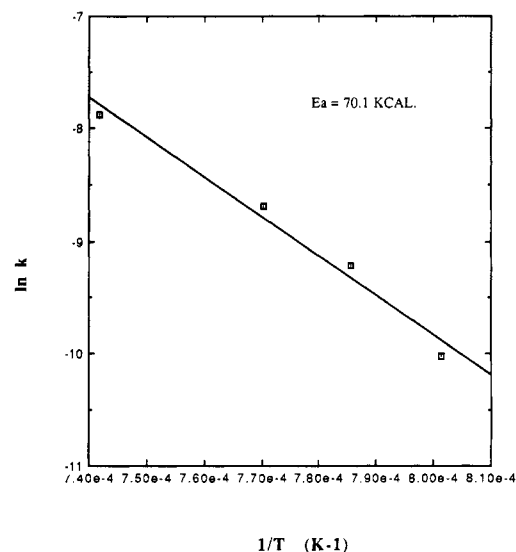


Figure 5. Arrhenius plot of mean rate constants for the formation of  $\text{Mg}_2\text{Al}_4\text{Si}_5\text{O}_{18}$ .

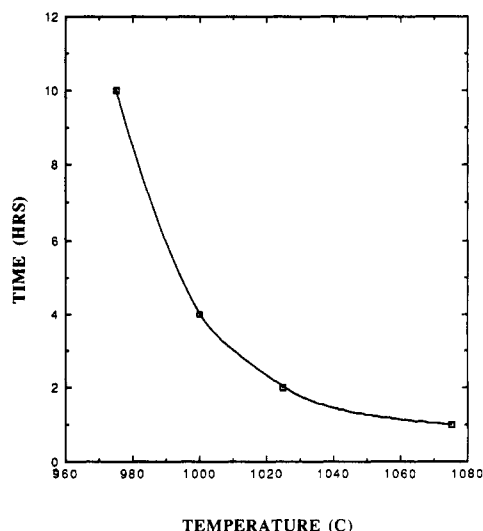
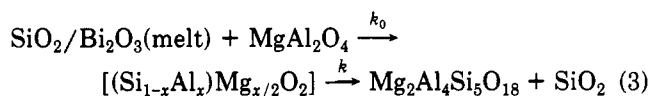


Figure 6. Induction period for the formation of  $\text{Mg}_2\text{Al}_4\text{Si}_5\text{O}_{18}$  as a function of temperature.

stants for  $\text{Mg}_2\text{Al}_4\text{Si}_5\text{O}_{18}$  appearance at different  $2\theta$  are generally in good agreement. The temperature dependence of the rate data appears in Figure 5. The measured ac-

tivation energy is 70 kcal/mol assuming an Arrhenius behavior.

The temperature dependence of the induction period for the appearance of  $\text{Mg}_2\text{Al}_4\text{Si}_5\text{O}_{18}$  is also shown graphically in Figure 6. This curve has a roughly exponential shape, with induction period decreasing with temperature. It was previously determined that below 960 °C this reaction does not proceed; that is, the induction period goes to a very large value at 960 °C. These two observations have some mechanistic implications for this reaction. A likely reason that the reaction to make cordierite does not proceed below 960 °C is that the bismuth silicate eulytite ( $\text{Bi}_4(\text{SiO}_4)_3$ ) melts between 955 and 960 °C. With an excess of  $\text{SiO}_2$  present it is expected that all the bismuth is tied up as this phase in the solid state. The exponential decrease in induction period with temperature is also consistent with the picture of a bismuth silicate flux acting as a reactive solvent in the reaction. Viscosity and diffusion are both exponential functions of temperature,<sup>11</sup> and thus a reaction that relied on the transport through a flux to proceed would be expected to display an induction period that decreased exponentially with increasing temperature, as this one does. There is also evidence that the flux is bismuth and silica rich. Where  $\text{SiO}_2$  is left out of the reaction, there is no effect on  $\text{MgAl}_2\text{O}_4$  by bismuth oxide alone. On the other hand, bismuth oxide is effective at crystallizing the amorphous  $\text{SiO}_2$  to  $\beta$ -cristobalite. Thus it is our conclusion that the induction period is due to the dissolution of  $\text{MgAl}_2\text{O}_4$  in the bismuth silicate flux and the diffusion required to make a suitably substituted silicate precursor to crystallize to  $\text{Mg}_2\text{Al}_4\text{Si}_5\text{O}_{18}$ :



The distribution of intermediates in this system is somewhat different from either the case of sol-gel or glass ceramic prepared cordierite. Both the crystallization of a glass and the crystallization of hydrolyzed precursors with the cordierite composition show the formation of a modified, substituted quartz<sup>7,8</sup> as an intermediate. This quartz solid solution is described as an aluminum-substituted  $\text{SiO}_2$  with magnesium in the channels to compensate for the excess negative charge. This modified hexagonal quartz has a wide compositional range around the cordierite composition with cell parameters varying smoothly with composition. The reaction described here appears to have this substituted quartz as an intermediate. This intermediate quartz does not, however, appear to be of the cordierite composition. The observed intermediate has reflections essentially identical with a hexagonal, substituted quartz<sup>10</sup> with cell parameters of  $a = 5.006 \text{ \AA}$  and  $c = 5.459 \text{ \AA}$ . These cell parameters match very well with

those of a quartz solid solution from ref 1 measured at 750 °C with aluminum and magnesium content of roughly half of  $\text{Mg}_2\text{Al}_4\text{Si}_5\text{O}_{18}$ , which is to say it is very  $\text{SiO}_2$  rich. This is consistent with the dynamic X-ray measurements where less than half the  $\text{MgAl}_2\text{O}_4$  disappears in the early stages of the reaction where the intermediate forms (Figure 3). There is also a second, more abundant intermediate that appears in this reaction that does not appear in the other glass ceramic prepared cordierite. This intermediate indexes as  $\beta$ -cristobalite. It seems unlikely that this is a reactive intermediate on the reaction path to cordierite.

The mechanism by which  $\text{MgAl}_2\text{O}_4$  and  $\text{SiO}_2$  convert to  $\text{Mg}_2\text{Al}_4\text{Si}_5\text{O}_{18}$  in the presence of the bismuth oxide flux thus appears to be a complex one. The initial disappearance of the  $\text{MgAl}_2\text{O}_4$  is consistent with its dissolution in the flux. The bismuth oxide containing flux likely is quite rich in  $\text{SiO}_2$ , as the lower temperature limit of this process of 960 °C suggests the melting of eulytite,  $\text{Bi}_4(\text{SiO}_4)_3$ , which is in the range 955–960 °C. Thus the process stops below about 960 °C, where there is no melt present. The stuffed quartz is clearly implicated in the conversion of starting materials to  $\text{Mg}_2\text{Al}_4\text{Si}_5\text{O}_{18}$ . In addition to being an intermediate in the aforementioned glass and sol-gel routes to  $\text{Mg}_2\text{Al}_4\text{Si}_5\text{O}_{18}$ , the stuffed quartz concentration reaches a maximum just before the appearance of crystalline cordierite in the X-ray powder pattern. As this modified quartz does not appear to be of the cordierite composition, then the crystallization products must be  $\text{Mg}_2\text{Al}_4\text{Si}_5\text{O}_{18}$  and free  $\text{SiO}_2$ . The other transient species, indexed as  $\beta$ -cristobalite, is likely not a reactive intermediate on the path to cordierite. On the contrary, the time-dependent X-ray data suggests that the formation of this crystalline species may inhibit the reaction. The initial disappearance of  $\text{MgAl}_2\text{O}_4$  and its subsequent reaction with  $\text{SiO}_2$  are believed to yield the stuffed quartz phase. The sharp decrease in the rate of spinel disappearance coincides with the appearance of crystalline  $\beta$ -cristobalite. This is also coincident with the plateau of the appearance of the stuffed quartz. The slowdown in the rate of reaction is likely due to the conversion of high surface area, reactive  $\text{SiO}_2$  to a low surface area crystalline form.

Structural analysis is in progress to determine the form of the cordierite (disordered and hexagonal or ordered and orthorhombic) and to locate bismuth in the final structure.

**Acknowledgment.** Thanks to Stefan Justi for his assistance with the hot-stage X-ray diffraction data collection. Special thanks to Angelica Stacy of UC Berkeley and Gary Wiseman of Raychem for helpful suggestions regarding the manuscript.

**Registry No.**  $\text{Mg}_2\text{Al}_4\text{Si}_5\text{O}_{18}$ , 12026-18-5;  $\text{SiO}_2$ , 7631-86-9;  $\text{MgAl}_2\text{O}_4$ , 12068-51-8; cordierite, 1302-88-1; bismuth oxide, 1304-76-3.